Biosensors and Bioelectronics 77 (2016) 901–906

Contents lists available at ScienceDirect

Biosensors and Bioelectronics

journal homepage: www.elsevier.com/locate/bios

A genetically encoded biosensor for *in vitro* and *in vivo* detection of $NADP^+$

Feng-Lan Zhao [a], Chang Zhang [a], Chen Zhang [b], Yun Tang [b], Bang-Ce Ye [a,*]

[a] Lab of Biosystems and Microanalysis, State Key Laboratory of Bioreactor Engineering, East China University of Science and Technology, 130 Meilong Road, Shanghai 200237, PR China

[b] Shanghai Key Laboratory of New Drug Design, School of Pharmacy, East China University of Science and Technology, 130 Meilong Road, Shanghai 200237, PR China

ARTICLE INFO

Article history:
Received 25 July 2015
Received in revised form
20 October 2015
Accepted 25 October 2015
Available online 26 October 2015

Keywords:
$NADP^+$
Computational protein redesign
FRET
Genetically encoded biosensor

ABSTRACT

$NADP^+$, the oxidized form of nicotinamide adenine dinucleotide phosphate, plays an essential role as a coenzyme in cellular electron transfer reactions. The concentration of $NADP^+$ in cytoplasm or organelles is dynamic due to its conversion to many important derivatives. To track the $NADP^+$ concentration in single living cells, we developed a genetically encoded $NADP^+$ biosensor by inserting a reporter element, ketopantoate reductase (KPR), between the Förster resonance energy transfer (FRET) pair, cyan fluorescent protein (CFP) and yellow fluorescent protein (YFP). This recombinant sensor showed a $NADP^+$ concentration-dependent decrease in the fluorescence ratio *in vitro* assay. In order to optimize this biosensor, we performed peptide-length optimization and site-directed mutagenesis in the binding pocket of KPR guided by predictions from computational protein redesign. This modified biosensor showed a 70% Δratio increase compared to the wild type and was found to be highly specific to $NADP^+$, with a detection limit of 1 μM. The sensor also reported $NADP^+$ real-time cellular dynamics in *Escherichia coli* (*E. coli*) after the addition of its precursor, nicotinic acid (NA). Altogether, these results demonstrate the feasibility of the biosensor for visualizing $NADP^+$ both *in vitro* and *in vivo*.

© 2015 Elsevier B.V. All rights reserved.

1. Introduction

$NADP^+$ is a key cofactor for electron transfer in the metabolism of all organisms (Berger et al., 2004; Pollak et al., 2007a; Xia et al., 2009). Numerous dehydrogenases depend on this pyridine nucleotide for vital physiological functions in processes such as pentose phosphate pathway and detoxification reactions (Kletzien et al., 1994; Shi and Shi, 2004). Additionally, $NADP^+$ serves as a precursor of potent calcium-mobilizing messengers (Agledal et al., 2010). A molecular tool to monitor the dynamics of cytosolic $NADP^+$ would help understanding signal transduction and cell metabolism. However, since the majority of the cellular $NADP^+$ is not free but bound to cytosolic proteins, the intracellular concentration of this small molecule is quite low (Canepa et al., 1991) and is thus difficult to evaluate. In the past decades, great efforts have been made to detect intracellular $NADP^+$ levels. Veech et al. (1969) determined the ratio of the [free $NADP^+$]/[free NADPH] in rat liver by measuring ratios of oxidized and reduced substrates of NADP-related dehydrogenase systems. This method is one of the few inchoate trials to focus on the change of free NADP in cytoplasm, but it just presents the ratio and not the dynamics of $NADP^+$ directly. High-performance liquid chromatography was also used to monitor $NADP^+$ through the general derivatization method (Norman and Pillai, 1996). This method is capable of quantitatively determining $NADP^+$ with high accuracy; however, it requires the use of cell extracts, and it cannot be used to study dynamics in intact individual cells. Until now, real-time tracking of $NADP^+$ can only be achieved by genetically encoded fluorescent biosensors.

Fluorescent biosensors have been developed to measure and visualize a large quantity of small signaling molecules and key metabolites in intact bacterial, plant or animal cells (Fehr et al., 2005; Medintz and Deschamps, 2006; Ponsioen et al., 2004; Zhang et al., 2013; Zhang and Ye, 2014b). Inspired by this, herein, we present a novel strategy for tracking $NADP^+$ in real-time by creating a genetically encoded fluorescent biosensor based on FRET. The efficiency of this energy transport depends on the fluorophore orientation and the distance between the donor and acceptor (Mitra et al., 1996). Ligand binding will induce a distance change between the two fluorophores and finally cause a change in FRET efficiency that can be directly measured through a

* Corresponding author. Fax: +86 21 64252094.
E-mail address: bcye@ecust.edu.cn (B.-C. Ye).

http://dx.doi.org/10.1016/j.bios.2015.10.063
0956-5663/© 2015 Elsevier B.V. All rights reserved.

fluorescence microplate reader. There have been efforts to develop FRET biosensors for central metabolites such as ATP, glutamate, maltose, ribose, glucose and N-(3-oxo-hexanoyl)-L-homoserine lactone (Fehr et al., 2002; Fehr et al., 2003; Imamura et al., 2009; Lager et al., 2003; Okumoto et al., 2005; Zhang and Ye, 2014b). Recently, we have developed a single fluorescent protein-based biosensor to trace the dynamic change of 2-oxoglutarate in *Escherichia coli* cells under various growth conditions that possessed larger singnal changes and faster kinetics compared with a formerly developed FRET-based biosensor (Zhang et al., 2013; Zhang and Ye, 2014a). The success of these developed biosensors had a great influence on the present work.

In this study, we designed a novel $NADP^+$ biosensor (NADPsor) consisting of an indicator protein KPR, and two fluorophores, CFP and YFP (Fehr et al., 2005). In the presence of $NADP^+$, the biosensor showed a concentration-dependent decrease in FRET efficiency. To improve the sensor sensitivity, we systematically engineered the lengths of *kpr* and performed site-specific mutagenesis on it and the obtained optimal link based on the result of computational protein redesign. The resulting biosensor was found to be highly specific to $NADP^+$ with a detection limit of 1 μM. This sensor was also employed to monitor the response of *E. coli* to the precursor of $NADP^+$, NA, and the obtained dynamic changes of FRET ratios demonstrated its competence for *in vivo* analysis of $NADP^+$.

2. Materials and methods

2.1. Reagents, bacteria strains and instruments

Chemical reagents, $NADP^+$, NADPH, NAD^+, NADH, NA, nicotinamide (NIA), kanamycin and isopropyl-β-D-thiogalactopyranoside (IPTG) were purchased from Sigma Aldrich (St. Louis, MO, USA). Restriction enzymes including *Bam*HI, *Eco*RI, *Sac*I and *Sal*I, T4 DNA ligase, and Phusion DNA polymerase, were purchased from TaKaRa Biotechnology Co., Ltd. (Dalian, China). The chemically competent *E. coli* DH5α and BL21 (DE3) strains and the site-directed mutagenesis kit were purchased from TransGen Biotech (Beijing, China). Fluorescence spectra were recorded by a fluorescence microplate reader Synergy™ Mx (Bio-Tek Instruments, Inc., Winooski, USA) using a black 96-well microplate (Fluotrac 200; Greiner Bio-One GmbH, Frickenhausen, Germany).

2.2. Plasmid construction

The gene encoding KPR (*NC_000913.2*) was amplified from genomic of *E. coli* by polymerase chain reaction (PCR). Four restriction sites, *Bam*HI, *Eco*RI, *Sac*I and *Sal*I, were chosen for the insertion of three genes, CFP, YFP and KPR, to construct the FRET-based biosensor. First, CFP was inserted into the pET-28a vector between *Sac*I and *Sal*I sites. Next, the second fluorescent protein YFP was inserted into the pET-28a vector between *Bam*HI and *Eco*RI sites. Finally, the reporting element KPR was inserted into the pET-28a vector between *Eco*RI and *Sac*I sites (Figs. S1 and S2). After this, the plasmid harboring the biosensor gene was inserted into the competent *E. coli* DH5α by heat shock and the bacteria were spread on the LB plate with 50 μg/mL kanamycin. Generally, *E. coli* DH5α was employed as the cloning host, and *E. coli* BL21 (DE3) was used as the protein production host.

2.3. Biosensor purification

E. coli BL21 (DE3) was grown at 37 °C in LB broth with 50 μg/mL kanamycin. When the optical density (OD_{600}) of culture reached 0.6, IPTG (0.5 mM) was added to induce protein expression and then cells were grown for an additional 12 h at 20 °C. Bacterial cells were harvested by centrifugation at 5000 rpm for 30 min, and the cell pellet was rinsed thrice before sonication using phosphate buffered saline (PBS) buffer (137 mM NaCl, 2.7 mM KCl, 10 mM Na_2HPO_4, 1.8 mM KH_2PO_4 at pH 8.0). A His-binding affinity chromatography resin column (Qiagen, Germany) was used for purification, with the resin first washed with 20 mM Tris–HCl, then 20 mM Tris–HCl containing 20 mM imidazole at pH 8.0, and finally being eluted with 250 mM imidazole in Tris–HCl (pH 8.0). The purified biosensor was dialyzed against PBS overnight at 4 °C to remove imidazole before *in vitro* assays.

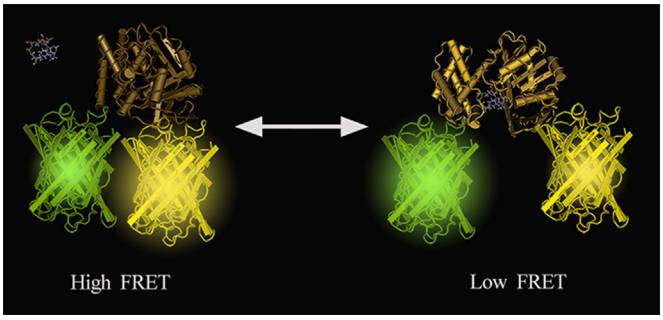

Fig. 1. Energy transfer illustration of NADPsor. In the $NADP^+$ free form (left), a closed conformation of KPR causes high FRET efficiency. In the $NADP^+$ bound form (right), the extended conformation of KPR decreases the FRET efficiency. The green, yellow, and brown structures represent CFP, YFP, and KPR, respectively, and the small molecule is $NADP^+$.

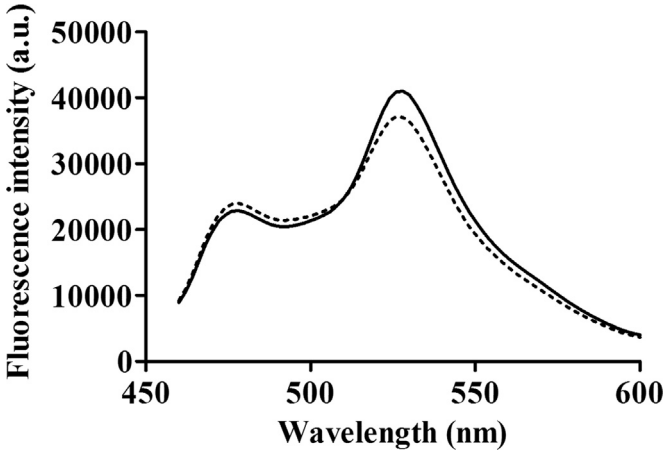

Fig. 2. Changes in the fluorescence emission spectrum of NADPsor with (dotted line) and without (solid line) $NADP^+$ after excitation at 440 nm.

2.4. In vitro assays

All *in vitro* assays were recorded by a fluorescence microplate reader in a black 96-well plate when excited at 440 nm with emission wavelengths of 478 and 526 nm or a continuous spectrum from 460 to 600 nm. FRET signal were recorded as the ratio change of 526/478. The blank was measured in a well containing only the biosensor without the addition of any chemical reagent. The affinity constants (K_d) were determined by fitting the titration curves to a single-site-binding isotherm: $R=R_{apo}+(R_{sat}-R_{apo})^*X/(K_d+X)$, where X is the ligand concentration, R is the ratio, R_{apo} is the ratio without ligand, and R_{sat} is the ratio with saturating ligand (Ewald et al., 2011). To guarantee reliability, all values were obtained by the averages of at least three titration experiments.

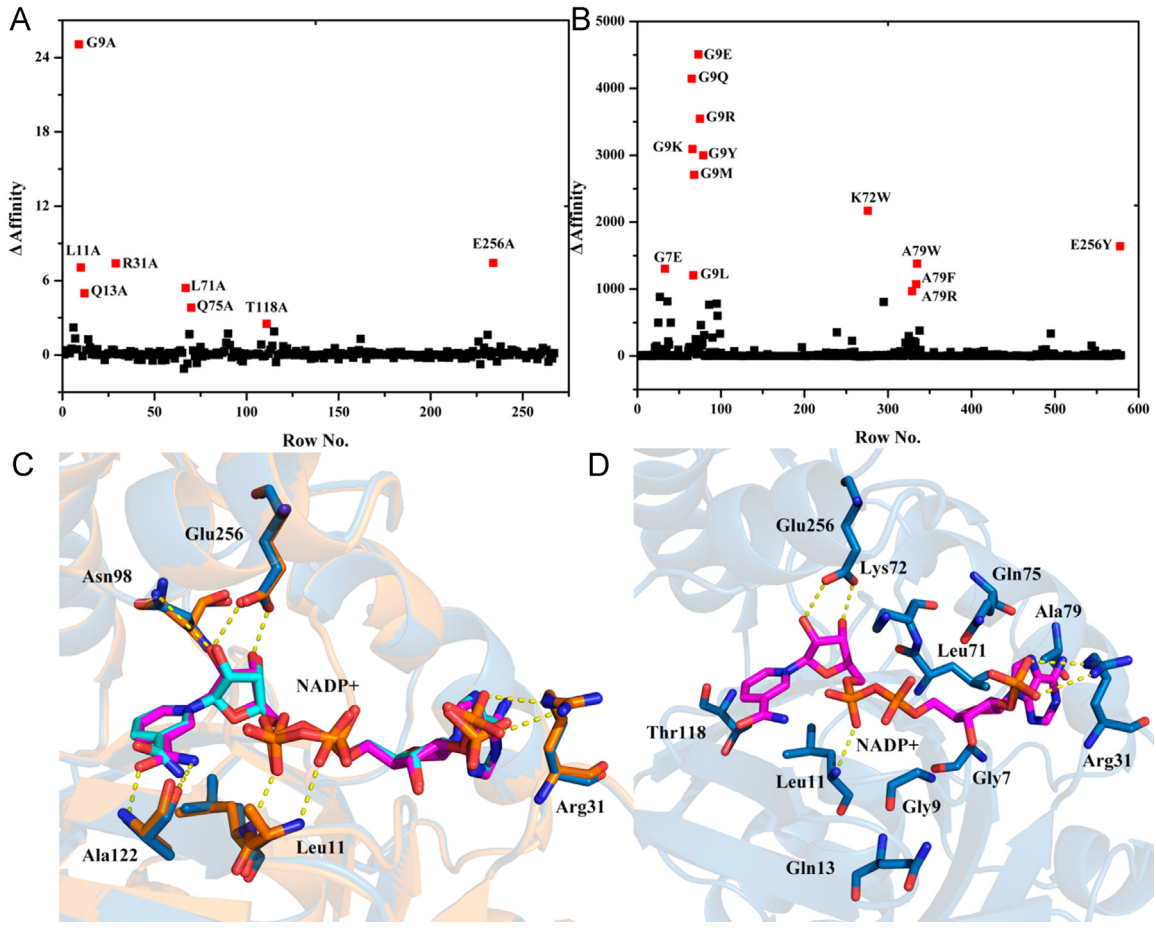

Fig. 3. Computational redesign of NADPsor. (A) Binding affinity changes with alanine scanning. (B) Binding affinity changes with specific mutations of residues within 5 Å of $NADP^+$. (C) Alignment of top 1 pose in docking study with KPR (PDB ID: 2OFP, chain A), RMSD 0.021. (D) Residues within 5 Å of $NADP^+$ selected for the residue scanning study.

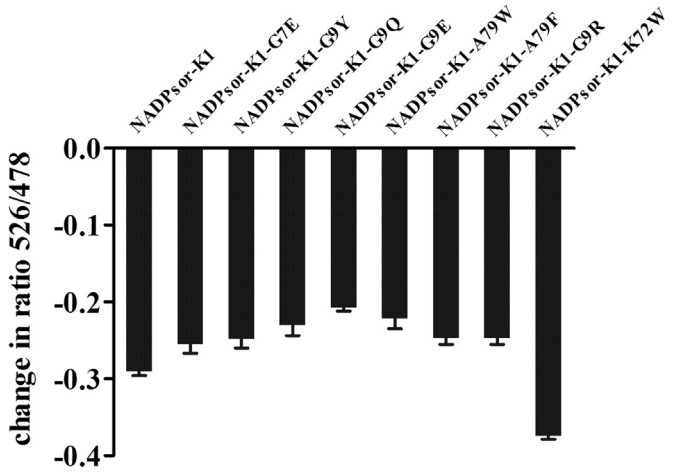

Fig. 4. Ratio changes of the NADPsors with 2 mM $NADP^+$. All sensors were adjusted to 0.3 mg/mL before detection.

2.5. *In vivo assay*

E. coli BL21 (DE3) was grown for 3 h in LB medium at 37 °C before induction by 0.5 mM IPTG. Next, cells were rinsed in carbon-free M9 medium (pH 8.0) and starved for 6 h. A volume of 200 μL of this culture was transferred to a 96-well plate, with NA or carbon-free M9 being added to the wells. The ratios before and after the addition of these compounds were recorded using a fluorescence microplate reader. Additionally, a $NADP^+$/NADPH quantification kit was used to detect $NADP^+$ change in single living cells at different times after the addition of NA or M9 buffer. Data were recorded as mentioned in the process of *in vitro* analysis (Section 2.4).

2.6. *Computational protein redesign*

The OPLS_2005 force field was used and the possible protonation states of $NADP^+$ at pH 5.0–9.0 were generated using Epik. KPR (PDB ID: 2OFP, chain A) was prepared using the "Protein Preparation Wizard" workflow in Schrödinger Suite. Bond orders were assigned and hydrogen atoms were added. The docking grid was generated using the "Receptor Grid Generation" center of $NADP^+$ with size less than 20 Å. Then, $NADP^+$ was docked to KPR using Glide 5.8 with extra precision (XP). At most, 5 poses were output with Epik state penalties set to docking score and other parameters were default. Finally, the top 1 pose of $NADP^+$ was kept and treated as the rationally binding pose. Furthermore, Ala scanning of all residues was calculated using residue scanning in Bioluminate module of Schrödinger Suite. Residues of 5 Å around $NADP^+$ were also selected and mutated to all other 19 amino-acids. The refinement cutoff distance was set to 0 Å and implicit solvent minimization was chosen for MM-GBSA calculation.

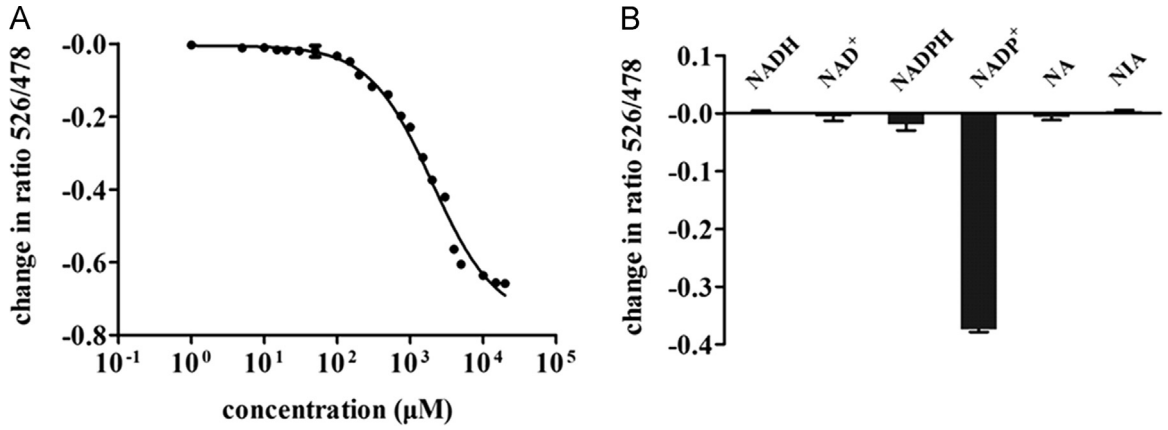

Fig. 5. Characterization of the NADPsor *in vitro*. (A) Binding curve of NDAP$^+$ to NADPsor. (B) FRET ratios of the biosensor with different ligands at 2 mM. Error bars indicate standard deviations (n=3).

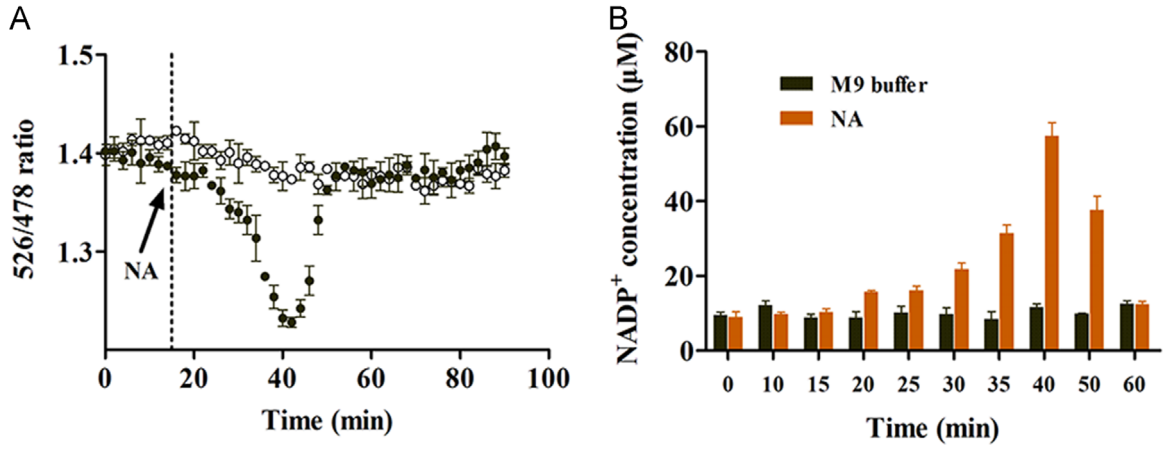

Fig. 6. (A) Real-time monitoring of the biosensor responding to NA (10 mM) in *E. coli*. NA was added at 15 min in the experimental group (black dots) while M9 buffer was added into the control group (white dots). (B) NADP$^+$ concentration in single living cells at different times after the addition of NA or M9 buffer. Error bars indicate standard deviations (n=3).

3. Results and discussion

3.1. Design and characterization of the biosensor

Previous studies reported that NADP$^+$ is capable of binding to the active site cleft between the N-terminal Rossmann-fold domain and the C-terminal R-helical domain of KPR and that this binding resulted in intriguing domain movements (Lobley et al., 2005; Matak-Vinkovic et al., 2001). Based on this, KPR was selected as a reporter element for the FRET-based biosensor. The initial design of the biosensor was composed of the mature length of the KPR domain sandwiched by CFP and YFP. As represented in Fig. 1, the binding of NADP$^+$ to KPR converts the protein from a relatively closed conformation into an open one. This conformational change further widens the distance between the two fluorescent molecules, and weakens the energy transfer from CFP to YFP. To quantify the FRET efficiency, *E. coli* cells harboring the NADPsor were cultured and the purified biosensor was obtained. When excited at 440 nm, the biosensor showed two peaks at 478 nm and 526 nm in the emission spectra corresponding to YFP and CFP (Fig. 2). The addition of NADP$^+$ caused an increase in CFP emission and a decrease in YFP emission. The 526/478 ratio changes responded to different concentrations of NADP$^+$ added, showing that the ratio change could be quantitatively correspond to the concentration change of NADP$^+$. Additionally, NADP$^+$ had little effect on YFP alone or CFP alone and did not influence the ratio change of the pair YFP–CFP without KPR, demonstrating it was NADP$^+$ binding to KPR that caused the conformational change and further weakened energy transfer (Fig. S3). Besides, the biosensor concentration only influenced the fluorescence intensity but not the 526/478 ratio changes (Fig. S4). These results demonstrate the sensor's feasibility for detecting NADP$^+$.

The initial biosensor, NADPsor-K, employed the wild type KPR domain. To determine the K_d of this sensor, NADP$^+$ at different concentrations was added into the reaction buffer, and the data recorded were fitted into a single site-binding curve as described in Section 2.4. Additionally, a panel of related metabolite compounds structurally similar to NADP$^+$, including NADPH, NAD$^+$, NADH, NA, and NIA, was chosen to test the selectivity of the biosensor. Nevertheless, the K_d of NADPsor-K was found to be 4 mM, which was too high for the intended applications and the biosensor failed to distinguish NADP$^+$ from NADPH (Fig. S5A and S5B). To construct a more effective sensor, we created a library of peptide linkers with different lengths. However, most of them were induced and expressed as inclusion bodies, indicating that large changes in protein structure may affect correct folding. Fortunately, NADPsor-K1 exhibited a ratio increase of about 30% compared with NADPsor-K and its detection range was 0.1–20 mM (Fig. S5C and S5D). NADPsor-K1 was an improvement on the initial biosensor, but the detection limit of NADPsor-K1 for NADP$^+$ was 100 μM. Considering that the concentration of free NADP$^+$ in the cytosol is estimated to be very low, the sensitivity of the sensor needs to be further improved.

3.2. NADPsor optimization

To obtain a highly sensitive sensor, we applied computational protein redesign approaches to improve the binding affinity of $NADP^+$ to KPR. The molecular docking study yielded the topmost docking pose of $NADP^+$ with docking score as 17.96, and the RMSD to $NADP^+$ was 0.021. The binding mode of $NADP^+$ in KPR and alignment of the top 1 docking pose with KPR are shown in Fig. 3C. After docking, the top 1 docking pose was used as the original complex structure for residue scanning studies. The binding affinity to each virtual mutant was calculated during the residue scanning studies. The results of the binding affinity changes of each point residue are shown in Fig. 3A and B. Finally, G7E, G9E, G9Q, G9R, G9Y, G9M, G9K, K72W, A79F, A79W, A79R and E256Y mutations were selected as the most promising for improving the binding of $NADP^+$ to KPR (Fig. 3D).

Based on these computational studies, we performed site-directed mutagenesis in the binding pocket of the intact length KPR and the shortened one K1 to generate biosensors with binding affinities capable of overlapping the physiological concentration of $NADP^+$. Not all of these mutants were successfully characterized, since some aborted during the expression process, some failed to distinguish $NADP^+$ from other molecules, and many more did not show any advantages compared with the wild type (Fig. 4). However, the NADPsor-K1-K72W sensor stood out with a lower K_d (2 mM) and a lower detection limit (1 μM), which indicates that the K72W mutation may be essential for substrate binding. Although the K_d of the senor exceeds the intracellular $NADP^+$ concentration, it still exhibits a detectable ratio change in the presence of 1 μM $NADP^+$ (Fig. 5A). Meanwhile, the computational protein redesign results have certain predictability. The selectivity test was also applied to the optimized NADPsor. Fig. 5B shows the ratio change of 526/478 after 10 min incubation, and $NADP^+$ produced an obvious ratio change while there was no detectable change for other ligands. The results clearly demonstrated that this novel biosensor can specifically recognize $NADP^+$ even in the presence of other cofactors with similar structures.

3.3. $NADP^+$ in vivo sensing

A significant advantage of biosensors is the ability to collect real time data to study the kinetics of metabolite variation. In this study, we detected intracellular $NADP^+$ in *E. coli* cells to verify the capabilities of NADPsor. $NADP^+$ plays a central role in the maintenance of a reducing equivalents pool for metabolic systems. The pathway known to yield $NADP^+$ is the phosphorylation of NAD^+ by NAD kinase (Burch et al., 1967; Pollak et al., 2007b). Generally, living cells use NA (vitamin B3) to generate NAD^+ and $NADP^+$ (Sauve, 2008). In this work, we monitored the dynamics of $NADP^+$ levels in *E. coli* cells after the addition of NA. Fig. 6A shows the time-dependent change of the emission ratio in the presence of 10 mM NA. *E. coli* was first incubated at 37 °C for 15 min, and after the addition of NA, the test group exhibited a time-dependent ratio decrease in the first 25 min and a rapid ratio increase in the next 10 min, whereas there was no detectable change in the control group. The addition of NA caused an obvious decrease in the ratio, indicating *E. coli* cells were capable of transforming NA to $NADP^+$, but the maintenance of the NADP pool was important to keep normal physiological metabolism, and ratio increase was recorded afterwards corresponding to $NADP^+$ being converted to NADPH or other compounds. The consumption of $NADP^+$ made the 526/478 ratio rebound and this change also certified the reversibility of the NADPsor. Additionally, a $NADP^+$/NADPH quantification kit was applied to determine $NADP^+$ in single living cells. This kit is specific for $NADP^+$ and NADPH, and the $NADP^+$ level can be obtained by $NADP_{total}$ ($NADP^+$ and NADPH) minus the amount of NADPH. Comparing Fig. 6A and B, a good consistency between the 526/478 ratio and the *in vivo* $NADP^+$ concentration was achieved. The result indicates that our proposed method is capable of monitoring *in vivo* $NADP^+$.

4. Conclusion

In summary, we have developed a novel method to measure intracellular $NADP^+$ levels based on the application of a genetically encoded biosensor. The biosensor possesses a number of unique features. First, it is capable of monitoring the dynamic change of $NADP^+$ in single living cells without the time-consuming procedure of extraction. Second, it offers an excellent specificity by recognizing $NADP^+$ from many other compounds with similar structure. Third, the biosensor has a broad detection range from 1 μM to 10 mM. Moreover, with the attachment of a proper signal sequence, NADPsor could potentially be able to monitor $NADP^+$ levels in other intracellular compartments such as animal cytosol or mitochondria and further facilitate biological research.

Acknowledgments

This work was jointly supported by the National Natural Science Foundation of China (21335003, 21421004, and 21276079), the Key Grant Project of Chinese Ministry of Education (313019), and the Fundamental Research Funds for the Central Universities.

Appendix A. Supplementary material

Supplementary data associated with this article can be found in the online version at http://dx.doi.org/10.1016/j.bios.2015.10.063.

References

Agledal, L., Niere, M., Ziegler, M., 2010. Redox Rep. 15, 2–10.
Berger, F., Ramırez-Hernandez, M.H., Ziegler, M., 2004. Trends Biochem. Sci. 29, 111–118.
Burch, H.B., Bradley, M.E., Lowry, O.H., 1967. J. Biol. Chem. 242, 4546–4554.
Canepa, L., Ferraris, A.M., Miglino, M., Gaetani, G.F., 1991. BBA – Gen. Subj. 1074, 101–104.
Ewald, J.C., Reich, S., Baumann, S., Frommer, W.B., Zamboni, N., 2011. PLoS One 6, e28245.
Fehr, M., Frommer, W.B., Lalonde, S., 2002. Proc. Natl. Acad. Sci. USA 99, 9846–9851.
Fehr, M., Lalonde, S., Lager, I., Wolff, M.W., Frommer, W.B., 2003. J. Biol. Chem. 278, 19127–19133.
Fehr, M., Okumoto, S., Deuschle, K., Lager, I., Looger, L., Persson, J., Kozhukh, L., Lalonde, S., Frommer, W., 2005. Biochem. Soc. Trans. 33, 287–290.
Imamura, H., Nhat, K.P., Togawa, H., Saito, K., Iino, R., Kato-Yamada, Y., Nagai, T., Noji, H., 2009. Proc. Natl. Acad. Sci. USA 106, 15651–15656.
Kletzien, R.F., Harris, P.K.W., Foellmi, L.A., 1994. FASEB J. 8, 174–181.
Lager, I., Fehr, M., Frommer, W.B., Lalonde, S., 2003. FEBS Lett. 553, 85–89.
Lobley, C.M., Ciulli, A., Whitney, H.M., Williams, G., Smith, A.G., Abell, C., Blundell, T. L., 2005. Biochemistry 44, 8930–8939.
Matak-Vinkovic, D., Vinkovic, M., Saldanha, S.A., Ashurst, J.L., von Delft, F., Inoue, T., Miguel, R.N., Smith, A.G., Blundell, T.L., Abell, C., 2001. Biochemistry 40, 14493–14500.
Medintz, I.L., Deschamps, J.R., 2006. Curr. Opin. Biotechnol. 17, 17–27.
Mitra, R.D., Silva, C.M., Youvan, D.C., 1996. Gene 173, 13–17.
Norman, H.A., Pillai, P., 1996. Anal. Biochem. 237, 30–36.
Okumoto, S., Looger, L.L., Micheva, K.D., Reimer, R.J., Smith, S.J., Frommer, W.B., 2005. Proc. Natl. Acad. Sci. USA 102, 8740–8745.
Pollak, N., Dolle, C., Ziegler, M., 2007a. Biochem. J. 402, 205–218.
Pollak, N., Niere, M., Ziegler, M., 2007b. J. Biol. Chem. 282, 33562–33571.
Ponsioen, B., Zhao, J., Riedl, J., Zwartkruis, F., van der Krogt, G., Zaccolo, M., Moolenaar, W.H., Bos, J.L., Jalink, K., 2004. EMBO Rep. 5, 1176–1180.
Sauve, A.A., 2008. J. Pharmacol. Exp. Ther. 324, 883–893.
Shi, Y.J., Shi, Y., 2004. Trends Genet. 20, 445–452.
Veech, R.L., Eggleston, L.V., Krebs, H.A., 1969. Biochem. J. 115, 609–619.

Xia, W.L., Wang, Z., Wang, Q., Han, J., Zhao, C.P., Hong, Y.Y., Zeng, L.L., Tang, L., Ying, W.H., 2009. Curr. Pharm. Des. 15, 12–19.
Zhang, C., Wei, Z.H., Ye, B.C., 2013. Appl. Microbiol. Biotechnol. 97, 8307–8316.
Zhang, C., Ye, B.C., 2014a. Biosens. Bioelectron. 54, 15–19.
Zhang, C., Ye, B.C., 2014b. Bioprocess Biosyst. Eng. 37, 849–855.